Biomaterials 34 (2013) 3870–3881

Contents lists available at SciVerse ScienceDirect

Biomaterials

journal homepage: www.elsevier.com/locate/biomaterials

Lactoferrin-modified PEG-co-PCL nanoparticles for enhanced brain delivery of NAP peptide following intranasal administration

Zhongyang Liu [a], Mengyin Jiang [c], Ting Kang [a], Deyu Miao [c], Guangzhi Gu [a], Qingxiang Song [b], Lei Yao [b], Quanyin Hu [a], Yifan Tu [a], Zhiqing Pang [a], Hongzhuan Chen [b], Xinguo Jiang [a], Xiaoling Gao [b,**], Jun Chen [a,*]

[a] Key Laboratory of Smart Drug Delivery, Ministry of Education & PLA, School of Pharmacy, Fudan University, Lane 826, Zhangheng Road, Shanghai 201203, PR China
[b] Department of Pharmacology, Institute of Medical Sciences, Shanghai Jiaotong University School of Medicine, 280 South Chongqing Road, Shanghai 200025, PR China
[c] School of Pharmacy, Shandong University of Traditional Chinese Medicine, Jinan, Shandong 250355, PR China

ARTICLE INFO

Article history:
Received 5 December 2012
Accepted 1 February 2013
Available online 27 February 2013

Keywords:
Brain targeting
Lactoferrin
Nanoparticle
NAP
Alzheimer's disease
Intranasal administration

ABSTRACT

Development of effective non-invasive drug delivery systems is of great importance to the treatment of Alzheimer's diseases and has made great progress in recent years. In this work, lactoferrin (Lf), a natural iron binding protein, whose receptor is highly expressed in both respiratory epithelial cells and neurons is here utilized to facilitate the nose-to-brain drug delivery of neuroprotection peptides. The Lf-conjugated PEG-PCL nanoparticle (Lf-NP) was constructed via a maleimide-thiol reaction with the Lf conjugation confirmed by CBQCA Protein Quantitation and XPS analysis. Other important parameters such as particle size distribution, zeta potential and *in vitro* release of fluorescent probes were also characterized. Compared with unmodified nanoparticles (NP), Lf-NP exhibited a significantly enhanced cellular accumulation in 16HBE14o-cells through both caveolae-/clathrin-mediated endocytosis and direct translocation. Following intranasal administration, Lf-NP facilitated the brain distribution of the coumarin-6 incorporated with the AUC_{0-8h} in rat cerebrum (with hippocampus removed), cerebellum, olfactory tract, olfactory bulb and hippocampus 1.36, 1.53, 1.70, 1.57 and 1.23 times higher than that of coumarin-6 carried by NP, respectively. Using a neuroprotective peptide – NAPVSIPQ (NAP) as the model drug, the neuroprotective and memory improvement effect of Lf-NP was observed even at lower dose than that of NP in a Morris water maze experiment, which was also confirmed by the evaluation of acetylcholinesterase, choline acetyltransferase activity and neuronal degeneration in the mice hippocampus. In conclusion, Lf-NP may serve as a promising nose-to-brain drug delivery carrier especially for peptides and proteins.

1. Introduction

Alzheimer's disease (AD), a devastating neurodegenerative disorder characterized by cortical amyloidogenesis, loss of neurons particularly in those regions associated with cognitive functions [1], are now representing one of the largest and fastest growing area of unmet medical need [2,3]. Today, 36 million people worldwide are living with dementia, with numbers doubling every 20 years to 66 million by 2030, and 115 million by 2050 [4]. Neurotrophic biomacromolecules such as nerve growth factor (NGF), brain-derived neurotrophic factor (BDNF) and insulin have showed neuroprotective effects on neurodegenerative diseases, and represent promising therapeutics to the treatment of AD [5]. However, the challenge to their clinical application is that most of them are not orally bioavailable and the blood–brain barrier (BBB) greatly limits their penetration for action in the brain following parenteral administration [5].

Intranasal administration provides a non-invasive alternative to the brain delivery of bioactive agents which could bypass the BBB and allow direct access of the therapeutic substances to the brain. The advantages include its rich vasculature, large surface area and highly permeable membrane for rapid absorption and avoidance of first pass metabolism; in addition, this delivery route is needleless, maximizing patient comfort and compliance [6–8]; more importantly, part of the therapeutics even stem cells [9] absorbed nasally could be delivered directly to the central nervous system (CNS) within minutes along both the olfactory and trigeminal nerves [10]. Actually, non-invasive intranasal delivery of peptide therapeutics to treat AD has already been done successfully in humans with

* Corresponding author. Tel.: +86 21 51980066.
** Corresponding author.
E-mail addresses: shellygao1@yahoo.com.cn (X. Gao), chenjun_1974@yahoo.com.cn, chenjun@fudan.edu.cn (J. Chen).

0142-9612/$ – see front matter © 2013 Elsevier Ltd. All rights reserved.
http://dx.doi.org/10.1016/j.biomaterials.2013.02.003

demonstrated therapeutic benefits [11,12]. Despite these advantages, the nose-to-brain absorption of most biomacromolecules (peptides, proteins and DNA) was still quite low due to their limit permeability and high susceptibility to the nasal cavity environment [10]. One promising strategy to improve the nose-to-brain delivery of these agents is to encapsulate them in poly (ethylene glycol) (PEG)-coated nanoparticles.

Over the last decade, PEG-coated polyester nanoparticles have attracted increasing attention as a drug delivery system (DDS) due to their favorable biological properties. Besides their biocompatibility, biodegradability and long-circulating behavior, PEG-coated polyester nanoparticles are able to enhance drug interaction with the mucus barriers and protect it from biological and/or chemical degradation [13]. However, the system still has its drawbacks; the surface PEG chains could probably inhibit its interaction with cell surfaces [14]. A key mechanism to obtain higher nasal adsorption of nanoparticles is modifying the nanocarrier with biological ligands that with receptors highly expression in the nasal cavity.

Lactoferrin (Lf), a natural iron binding cationic glycoprotein of the transferrin family, weighs 80 kDa, consists of a single-chain glycoprotein folded into two globular lobes, is expressed in various tissues and involved in various physiological processes [15–18]. Extensive histological studies showed that Lf receptor (LfR) was highly expressed on the apical surface of respiratory epithelial cells [19], and also in the brain cells such as brain endothelial cells and neurons [20,21]. Besides, LfR has also been demonstrated to be overexpressed in the CNS associate with age-related neurodegenerative diseases including AD, Parkinson's disease, Huntington's disease and amyotrophic lateral sclerosis [22]. Furthermore, Lf has shown higher brain uptake than transferrin (Tf) and OX-26, an anti-Tf receptor antibody [23]. Based on this information, we speculated that Lf might serve as a suitable ligand for mediating enhanced nose-to-brain delivery of nanoparticles following intranasal administration.

NAP (NAPVSIPQ), an 8-amino acid neuropeptide fragment derived from the activity-dependent neuroprotective protein (ADNP) family, is currently in Phase II clinical trials, which showed neuroprotection effects at low concentration (ranging from 10^{-17} to 10^{-10} M), and considered as a promising candidate for the treatment of AD [24–26]. It exhibited neurotrophic/neuroprotective activity in various *in vitro* neuronal cell cultures, protecting cells against the neurotoxicity induced by β-amyloid, electrical blockade by tetrodotoxin and oxidative stress by hydrogen peroxide [27–29]. *In vivo* NAP protected animals against traumatic brain injury, oxidative stress and apolipoprotein E-deficiency-associated cholinergic dysfunction and learning/memory impairments [29–31]. However, the nasal absorption of NAP is still limited by its rapid enzymatic degradation by nasal cytochrome P450/peptidases/proteases, low permeability via the nasal mucosa and rapid mucociliary clearance [32].

Therefore, the aim of this study was to determine the potential of Lf-conjugated poly(ethyleneglycol)-poly (ε-caprolactone) nanoparticle (Lf-NP) for delivering neuroprotective agents to the treatment of AD. Fluorescently labeled nanoparticles were used to study the *in vitro* cellular interaction of Lf-NP and its *in vivo* biodistribution and brain targeting efficiency following intranasal administration. Using NAP as the model drug, neuroprotective effects of the Lf-NP formulation was evaluated in AD mice model.

2. Experimental

2.1. Materials

Methoxyl poly(ethylene glycol)-co-poly(ε-caprolactone) copolymer (Me-PEG-PCL, 15 kDa) and Maleimidyl-poly(ethylene glycol)-co-poly(ε-caprolactone) copolymer (Maleimide-PEG-PCL, 18 kDa) were kindly gifted by East China University of Science and Technology. Coumarin-6, Ibotenic acid (IBO), and β-amyloid$_{1-40}$ (Aβ$_{1-40}$) were purchased from Sigma–Aldrich (St. Louis, MO, USA). Mono-reactive hydroxysuccinimide ester of Cy5.5 (NHS-Cy5.5) was purchased from Amersham Bioscience (Piscataway, NJ, USA). DAPI (4, 6-diamidino-2-phenylindole) was obtained from Molecular Probes (Eugene, OR, USA). Penicillin-streptomycin, Dulbecco's modified Eagle's medium (high glucose) (DMEM), fetal bovine serum (FBS) and 0.25% (w/v) trypsin solution were purchased from Gibco BRL (Gaithersberg, MD, USA). NAP (NAPVSIPQ) was synthesized by the ChinaPeptides Co., Ltd (Shanghai, China). Quantity Protein assay kits, acetylcholinesterase (AChE) and choline acetyltransferase (ChAT) activity assay kits were purchased from Nanjing Jiancheng Bioengineering Institute (Nanjing, China). All the other chemicals were of analytical grades and used without further purification.

2.2. Cell line

16HBE14o-cells, human bronchial epithelial cell line, were cultured in DMEM medium, supplemented with 10% FBS, 100 IU/ml penicillin and 100 μg/ml streptomycin sulfate. All the cells were cultured in incubators at 37 °C, 5% CO_2.

2.3. Animals

Male ICR mice (4–5 weeks, 20 ± 2 g) and male SD rats (8–10 weeks, 220 ± 20 g) were supplied by Department of Experimental Animals, Fudan University (Shanghai, China), and acclimated at 25 ± 1 °C, 55% of humidity under natural light/dark conditions for 1 week before experiment. All the animal experiments were carried out in accordance with guidelines evaluated and approved by the ethics committee of Fudan University (Shanghai, China).

2.4. Preparation and characterization of nanoparticles

2.4.1. Preparation of nanoparticles

Unmodified nanoparticles (NP) loaded with coumarin-6 or NAP were prepared respectively for different purposes using the emulsion/solvent evaporation technique [33]. For coumarin-6-loaded NP, MePEG-PCL (22.5 mg), Male-PEG-PCL (2.5 mg) and 0.1% (w/w) of coumarin-6 were dissolved in 1 ml dichloromethane, and then added with 50 μl of deionized water as inner phase of the w/o primary emulsion, which was produced by sonication (160 W, 30 s) on ice using a probe sonicator (Ningbo Scientz Biotechnology Co. Ltd., China). The primary emulsion was then emulsified by sonication (220 W, 30 s) on ice in a 2 ml of 1% aqueous sodium cholate solution. The resulted w/o/w emulsion was further diluted into 8 ml of a 0.5% aqueous sodium cholate solution and then stirred for 5 min at room temperature. After that, the organic solvent was evaporated by a ZX-98 rotavapor (Shanghai Institute of Organic Chemistry, China). The formed nanoparticles were concentrated by centrifugation at 15,000 rpm for 45 min using a TJ-25 centrifuge (Beckman Counter, USA) at 4 °C. After the supernatant discarded, the pellets were resuspended in 2 ml HEPES buffer (pH 7.0) and purified with a 1.5 × 20 cm Sepharose CL-4B column (Pharmacia Biotech, Inc., Sweden). The nanoparticles loaded with NAP were prepared with the same way using 50 μl of NAP solution (25 mg/ml) as the inner phase of the primary emulsion. All the procedures were conducted in darkness.

2.4.2. Preparation of lactoferrin-conjugated nanoparticles

Lf was thiolated by reaction for 60 min with a 40:1 M excess of 2-iminothiolane (Traut's reagent) according to Huwyler's method [34]. The product was desalted with a Hitrap™ Desalting column (Amersham Pharmacia Biotech AB, Sweden). The amount and stability of the introduced thiol groups were determined spectrophotometrically (λ = 412 nm) with Ellmann's reagent [35]. The maleimide-functionalized nanoparticles were reacted with the purified thiolated Lf via a maleimide-thiol coupling reaction in HEPES buffer (pH 7.0) at room temperature for 9 h. The product was then subjected to a 1.5 × 20 cm sepharose CL-4B column and eluted with 0.01 M HEPES buffer (pH 7.0) to remove the unconjugated protein.

2.4.3. Morphology, particle size and zeta potential

The morphological examinations of nanoparticles were studied by transmission electron microscopy (TEM) (H-600, Hitachi, Japan) after negative staining with sodium phosphotungstate solution (2%, w/v). The average size and zeta potential of the nanoparticles were determined with a Zetasizer Nano ZS (ZEN3600, Malvern Instruments).

2.4.4. Lf conjugation efficiency, Lf density on nanoparticle surface and X-ray photo electron spectroscopy

The Lf conjugation efficiency (CE) was determined via a CBQCA Protein Quantitation Kit (Molecular Probes), a rapid and highly sensitive method for the quantitation of peptides and proteins. The calculation formula is as follow: CE (%) = (amount of Lf conjugated to the nanoparticle surface/total amount of Lf added) × 100%.

The average Lf number on each nanoparticle was calculated by dividing the number of Lf molecules by the calculated average number (n) of nanoparticles using the methods described previously [36]: $n = 6m/(\pi \times D^3 \times \rho)$ (m, the nanoparticle

weight; D, the number-based mean nanoparticle diameter determined by DLS; ρ, the nanoparticle weight per volume unit (density), estimated to be 1.1 g/cm^3 [37].

In order to determine the surface composition of NP and Lf-NP, the samples were lyophilized using an ALPHA 2-4 Freeze Dryer (0.070 Mbar Vakuum, −80 °C Martin Christ, Germany) and subjected to X-ray photo electron spectroscopy (XPS) analysis. The determination was performed via an RBD upgraded PHI-5000C ESCA system (Perkin Elmer).

2.4.5. Encapsulation efficiency and loading capacity

To determine the encapsulation efficiency (EE) and loading capacity (LC) of NAP-loaded Lf-NP (Lf-NP-NAP), the nanoparticles were dissolved in acetonitrile. After centrifugation at 12,000 rpm for 10 min, concentration of NAP in supernatant was measured via an HPLC system (Shimadzu LC-10A VP system, Kyoto, Japan) for analysis. Analyses were performed on an YMC® ODS-A reverse phase column (5 μm particle size, 150 mm × 4.6 mm i.d., YMC Co., Ltd., Kyoto, Japan). The mobile phase was composed of 0.1% (V/V) trifluoroacetic acid in acetonitrile: 0.1% trifluoroacetic acid in water = 15:85. The column effluent was detected with a UV/VIS detector at 225 nm. The flow rate was set at 1.2 ml/min, and the column was maintained at 40 °C. The retention time of NAP was about 10 min. The calibration curve was linear in the range of 5–500 μg/ml with a correlation coefficient of $R^2 = 0.999$. EE was defined as the ratio between actual NAP amount detected and theoretic feeding NAP amount and LC was defined as the ratio between detected NAP amount and the weight of polymers.

2.5. Cellular uptake of coumarin-6-labeled NP and Lf-NP in 16HBE14o-cells

Qualitative analysis of cellular association of Lf-NP was performed via fluorescent microscopy. 16HBE14o-cells were seeded in a 48-well plate at the density of 2×10^4 cells/well. On the second day, the cells were incubated with coumarin-6-loaded NP and Lf-NP at different concentrations at 37 °C for 1 h. After that, the cells were washed three times with PBS and fixed with 4% formaldehyde for 10 min. After stained with 100 ng/ml DAPI for 10 min, the cells were washed three times with PBS and observed under a fluorescent microscope (Olympus, Japan).

Quantitative analysis of the cellular uptake was conducted using a high content analysis system [38,39]. 16HBE14o-cells were plated on a 96-well plate at the density of 5×10^3 cells/well. On the second day, the cells were incubated with coumarin-6-loaded Lf-NP and NP (5–800 μg/ml) for 1 h at 4 °C and 37 °C, respectively. After that, the cells were washed three times with PBS and fixed with 4% formaldehyde for 10 min. Away from light, the cells were stained with 10 μg/ml Hochest 33258 (Pentahydrate (bis-Benzimide), a nucleic acid stain) at room temperature for 10 min. Finally, the cells were washed for three times and detected under a KineticScan® HCS Reader (version 3.1, Cellomics Inc., Pittsburgh, PA, USA). To study the effects of incubation time on nanoparticle uptake, the cells were incubated with the nanoparticles (200 μg/ml) at 37 °C for 0.25, 0.5, 1, 2, 3 and 4 h, respectively. For determining the level of cellular internalized nanoparticles, the cells were incubated with trypan blue (Beyotime Institute of Biotechnology) to quench those fluorescent signals from the uninternalized ones, and subjected to a second high content analysis system analysis.

The mechanism of cellular internalization was further evaluated via endocytosis inhibition experiments. Prior to incubation with Lf-NP (90 μg/ml, 1 h, 37 °C), the cells were preincubated with Lf (1 mg/ml) and other endocytic inhibitors (10 μg/ml chlorpromazine, 4 μg/ml colchicines, 5 μg/ml filipin, 10 μg/ml cyto-D, 200 nM monensin, 10 mM NaN_3 + 50 mM deoxyglucose, 20 μM Nocodazole, 5 μg/ml BFA and 100 mM Genistein) for 30 min, respectively. Quantitative analysis of the cellular uptake following the inhibitor treatments was performed as mentioned above and compared with that of the non-inhibited control.

2.6. Brain delivery of Lf/Lf-NP following intranasal administration

2.6.1. Brain distribution of Cy5.5-labeled Lf after intranasal administration

In vivo real-time fluorescence imaging analysis was used to study the brain distribution of Lf following nasal administration. For the experiment, Lf and bovine serum albumin (BSA) were fluorescently labeled by reacting with Cy5.5 according to the manufacturer's recommendations at a final protein/dye ratio at 1. Labeling was started by mixing 1 ml of protein (0.5 mg/ml in Sodium Carbonate-Sodium Bicarbonate buffer) with 10 μL of Cy5.5/DMSO solution. After incubated at room temperature for 1 h, the labeled Lf/BSA was purified with an ultrafiltration unit (Millipore, MW cut off 3 kDa) to remove the excess, unconjugated dye.

Before administration, SD rats were anesthetized by intraperitoneal injection of chloral hydrate, and then fixed in a supine position. One group of the animals ($n = 3$) were nasally administrated with Cy5.5-labeled Lf and the other with Cy5.5-labeled BSA at the dose of cy5.5 0.5 mg/kg (10 μl/nostril). For administration, conscious animals were fixed in a prostrate position, and the preparations were given at the openings of the nostrils via a polyethylene 10 (PE 10) tube attached to a microlitre syringe. The procedure lasted about 3 min, allowing the animal to inhale all of the preparations. At predetermined time points post-administration, the rats were anesthetized and detected under a Maestro *in vivo* imaging system (CRI, MA). To compare the tissue distributions of Cy5.5-labeled Lf, the rats were sacrificed at 3 h post-administration with the brains, hearts, livers, spleens, lungs and kidneys harvested, washed with saline and subjected to imaging under the Maestro *in vivo* imaging system.

2.6.2. Brain distribution of coumarin-6-labeled NP and Lf-NP following intranasal administration

For quantitative studies, thirty-six SD rats were divided into two groups: one group intranasal administrated with unconjugated coumarin-6-loaded NP, and the other Lf-NP. Each animal received a total of 20 μl nanoparticles (10 μl each nostril) containing 5 μg coumarin-6. At each predetermined time points (0.25, 0.5, 1, 2, 4 and 8 h), the animals were euthanized with blood collected. After that, the animals were heart perfused with 60 ml cold saline with the brain removed and excised into cerebrum with hippocampus removed, cerebellum, olfactory tract, olfactory bulb and hippocampus.

To determine the accumulation of coumarin-6 in the CNS, the tissue samples were treated and subjected to liquid chromatography-tandem mass spectrometry (LC-MS/MS) analysis as described previously [40]. The coumarin-6 concentrations were dose-normalized and plotted as concentration-time curves. Drug and Statistics software (DAS ver 2.1.1) was utilized to calculate the pharmacokinetic parameters.

2.7. Neuroprotective effect of Lf-NP-NAP in mice co-injection with $A\beta_{1-40}$ and IBO

2.7.1. $A\beta_{1-40}$ and IBO co-injection model

$A\beta_{1-40}$ was dissolved in saline (2 μg/μl) and allowed to aggregate by incubation at 37 °C for 7 days. Before surgery, same aliquot of $A\beta_{1-40}$ and IBO solutions (dissolved in saline, 1 μg/μl) were mixed to a final concentration of $A\beta_{1-40}$ 1 μg/μl and IBO 0.5 μg/μl. Male ICR mice were anaesthetized with chloral hydrate and then mounted on a stereotactic device equipped with a mouse adaptor. The animals were bilaterally injected in the dorsal hippocampus through a microsyringe with 5 μl of the mixture of $A\beta_{1-40}$ and IBO or same volume of saline over 6 min, at the following coordinates: 2.3 mm posterior to the bregma, ±1.8 mm lateral to the midline and 2.0 mm ventral to the skull surface.

2.7.2. Morris water maze (MWM) task

Four days after the co-injection of $A\beta_{1-40}$ and IBO, the mice were divided into eight groups ($n = 8$), and received daily intranasal administration of saline (AD control and sham control), NAP solution (NAP, 0.05 μg/mouse/d and 0.1 μg/mouse/d, respectively), NP-NAP (NAP, 0.05 μg/mouse/d and 0.1 μg/mouse/d, respectively) or Lf-NP-NAP (NAP, 0.05 μg/mouse/d and 0.1 μg/mouse/d, respectively).

Thirty days later, cognitive performance assessment – MWM tasks were carried out 1 h following drug administration for 5 days. The MWM setting consisted of a circular pool (diameter, 150 cm; height, 50 cm) equipped with a 9-cm platform 1 cm below the surface of the opacified water (30 cm deep) in the middle of a quadrant. On the first four days, the mice were tested four times from four different positions around the border of the maze in a semi-random order with 90 s latency to reach the platform. If the animal succeeded to find the hidden platform within 90 s, it was allowed to remain on the platform for 15 s. If it failed, the animal had to be placed on the platform for 15 s. The trajectory of each mouse was recorded and analyzed using a computerized video-tracking system.

The probe trails were performed on the fifth day with the platform removed from the pool. Each of the trained animal was allowed to swim freely for 60 s, with two starting points far away from the platform. The time each mouse spent looking for the platform in the quadrant where the platform used to be (target quadrant), and the number of times it crossed the former platform area were recorded.

2.7.3. AChE activity and ChAT activity in mice hippocampus

It was well established that the cholinergic neurotransmitter system, which is involved in cognitive process, was severely impaired by intrahippocampal injection of $A\beta_{1-40}$ and IBO solution [41–43]. Hereto, AChE activity and ChAT activity in mice hippocampus were determined at the termination of the behavioral experiments as described previously ($n = 5$) [44]. Protein concentrations were determined using a Quantity Protein assay kit.

2.7.4. Histology

At the end of the behavioral studies, hematoxylin/eosin (HE) staining and Nissl staining were used to examine the histology of brain with light microscopy. Histologic evaluation was performed on formalin-fixed paraffin-embedded sections: three mice from each group were euthanized, followed by heart perfusion with 60 ml of cold saline. The whole brains were harvested and fixed in 10% formalin, embedded in paraffin, sectioned at 5 μm and stained with Nissl or hematoxylin/eosin following standard protocol. For histological studies, all histopathological tests were performed using standard laboratory procedures. The sections were observed under a microscope and photographed. Nissl staining sections were used for quantitative analysis of neuronal injury in the CA1 region of hippocampus. Cell counts were performed in 5 randomly assigned regions of interest (450 μm × 550 μm) in each animal ($n = 3$) by using the optical dissector method [45].

2.8. Statistical analysis

All data were expressed as mean ± SD. For multiple-group comparison, one-way ANOVA was used followed by Bonferroni tests. Specific comparison between groups was carried out with an unpaired Student's t-test (two tailed). Differences were considered statistically significant at $p < 0.05$.

3. Results

3.1. Preparation and characterization of the nanoparticles

The physical characterizations of coumarin-6/NAP-loaded nanoparticles (NP-NAP) were shown in Table 1. The nanoparticles exhibited an average diameters 70–90 nm under transmission electron microscopy (Fig. 1), which was in good agreement with the number-based particle size measured by the laser scattering technique. A slight increase in volume-based mean diameters of Lf-NP was observed compared with that of the unmodified nanoparticles. The nanoparticles with or without Lf modification showed similar acceptably polydispersity indexes (PI < 0.25).

Under our experimental conditions (molar ratio of maleimide-PEG-PCL to Lf 1:1, incubation time for conjugation reaction 9 h), Lf conjugation efficiency was 22.6%, and Lf density on the nanoparticle surface was around 46. XPS analysis showed 0.32% nitrogen on the Lf-nanoparticle surface while none on the unmodified nanoparticles.

The EE and LC of NP-NAP and Lf-NP-NAP were 54.34 ± 3.02%, 47.61 ± 2.36%, and 0.71 ± 0.016%, 0.62 ± 0.013%, respectively.

3.2. Cellular uptake of coumarin-6-labeled NP and Lf-NP in 16HBE14o-cells

Cellular association of coumarin-6-labeled NP and Lf-NP in 16HBE14o-cells were qualitatively presented by fluorescent microscope images (Fig. 2). At all the detected concentrations, the cellular association of Lf-NP was much higher than that of NP.

Quantitative analysis revealed the time-dependent, temperature-dependent and concentration-dependent mode of cellular uptake of NP and Lf-NP (Fig. 3A and B). The cellular uptake of Lf-NP was significantly higher than that of NP at each time (1.91, 2.92, 3.46, 3.68 and 3.02 times of that of NP at 200 μg/ml after 0.5, 1, 2, 3 and 4 h incubation at 37 °C, respectively) (Fig. 3A), and at both 37 °C and 4 °C (at 37 °C, about 4.25, 4.75, 5.27, 6.39, 3.87 times higher than that of NP at the concentration of 200, 300, 400, 600 and 800 μg/ml, respectively; and at 4 °C about 7.32, 3.68, 9.63, 8.63 and 6.05 times higher than that of NP at the concentration of 200, 300, 400, 600 and 800 μg/ml, respectively).

Endocytosis inhibition experiments showed that the cellular uptake of Lf-NP was inhibited by chlorpromazine, filipin, NaN_3 + deoxyglucose and Genistein (Fig. 4), but not or less affected by other inhibitors including colchicines, cyto-D, monensin, Nocodazole and BFA. Besides, a significant reduction in the cellular uptake of Lf-NP was observed in the presence of excess Lf (Fig. 4).

3.3. Brain delivery of Lf/Lf-NP following intranasal administration

3.3.1. Brain distribution of Cy5.5-labeled Lf after intranasal administration

The fluorescent probe Cy5.5 allowed real-time imaging and tracking the biodistribution of Cy5.5-labeled Lf after intranasal administration (Fig. 5A). Compared with Cy5.5-labeled BSA, the fluorescence signal of Cy5.5-labeled Lf in the brain was much higher at all time points post-administration. Three hours post-administration, an obvious stronger fluorescent signal of Cy5.5-labeled Lf was observed in the brain compared with that of Cy5.5-labeled BSA (Fig. 5B). Besides, the labeled proteins were found mainly distributed in the liver, lung and kidney (Fig. 5C).

Table 1
Characterization of coumarin-6/NAP-loaded nanoparticles and lactoferrin-functionalized nanoparticles.

Formulation	Vesicle size (nm)	PI	Zeta potential (mV)
Coumarin-6-NP	73.2 ± 4.2	0.11 ± 0.013	−25.13 ± 0.98
Coumarin-6-Lf-NP	89.0 ± 5.7	0.20 ± 0.039	−23.08 ± 0.74
NP-NAP	76.2 ± 6.5	0.15 ± 0.020	−24.24 ± 0.81
Lf-NP-NAP	88.4 ± 7.8	0.22 ± 0.033	−23.56 ± 0.96

Data are represented with mean ± SD ($n = 3$).

3.3.2. Brain distribution of coumarin-6-labeled NP and Lf-NP following intranasal administration

The brain distribution of coumarin-6-labeled NP/Lf-NP was also quantitatively assessed in rats after intranasal administration. As shown in Fig. 6A, NP and Lf-NP showed similar plasma concentration-time curves, and the highest blood coumarin-6 concentration was achieved at 1 h after dosing (Table 2). In contrast, the brain concentration of coumarin-6 after intranasal administration of Lf-NP was significantly higher in all the five brain tissues compared with that of the unconjugated NP. The AUC_{0-8h} in the olfactory bulb, olfactory tract, cerebrum with hippocampus removed, cerebellum and hippocampus was 2.57, 2.70, 2.22, 2.70 and 2.23 times, respectively, when compared with that of the unconjugated NP (Fig. 6B–F). The AUC_{0-8h} ratio of brain tissues to blood (AUC_{brain}/AUC_{blood}) of coumarin-6 incorporated in Lf-NP was also much higher than that of coumarin-6 associated to the unmodified NP (2.69, 2.27, 3.80, 3.57 and 3.51 folds for the olfactory bulb, olfactory tract, cerebrum with hippocampus removed, cerebellum and hippocampus, respectively, Table 2).

3.4. Neuroprotective effect of Lf-NP-NAP in mice co-injected with $A\beta_{1-40}$ and IBO

3.4.1. Behavioral analysis of $A\beta_{1-40}$ and IBO co-injected mice

Neuroprotective effect of Lf-NP-NAP in mice co-injected with $A\beta_{1-40}$ and IBO were studied in an MWM. Latencies to find the hidden platform were measured daily (Fig. 7A). It was found that the AD control animals did not show shorten latency even after 4 days training progress, on the other hand, the sham control animals exhibited significantly shorter latency than AD control group on days 2, 3 and 4. Intranasal application of NAP formulations ameliorated cognitive deficits in a dose-dependent manner: daily intranasal administration of 0.1 μg NAP solution shortened latency on day 4 compared with AD control animals, while daily i.n. of 0.05 μg NAP solution group showed no significant difference. In the daily i.n. NP-NAP groups, the 0.1 μg NP-NAP group showed decreased latency compared with the 0.05 μg NP-NAP group. In the case of Lf-NP-NAP, significant decrease in latency was observed at the dose of 0.1 μg NAP on day 2, 3, and 4, but only on day 3 and 4 at the dose of 0.05 μg NAP. The same results were observed in the probe tests carried out on the fifth day of the test (Fig. 7B & C). The reduction in the number of times crossing the area where the platform had been located was significantly ameliorated in the i.n. NAP formulation groups: NP-NAP (0.1 μg/day); Lf-NP-NAP (0.05 μg/day) and Lf-NP-NAP (0.1 μg/day) (Fig. 7B). These outcomes were further confirmed by the percentage of time spent in the target quadrant (Fig. 7C). ANOVA analysis with Bonferroni adjustment for multiple comparisons showed significant differences between sham control and AD control; NP-NAP (0.1 μg/day) group and AD control; Lf-NP-NAP group (0.05 μg/day) and AD control as well as Lf-NP-NAP (0.1 μg/day) group and AD control.

3.4.2. AChE and ChAT activity in mice hippocampus

Both AChE and ChAT activity in mice hippocampus of the sham control and the NAP-treated groups were significantly different with that in the AD control animals ($p < 0.05$) (Fig. 8A & B). The NAP-treated groups exhibited a reduction in AChE activity, which ameliorated the dysfunction of cholinergic neurotransmitter

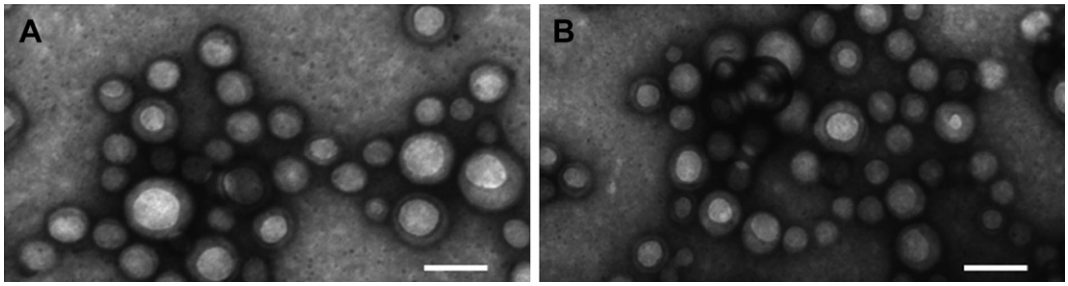

Fig. 1. Transmission electron micrographs of (A) NP and (B) Lf-NP. Bar = 100 nm.

system. In the case of ChAT, the Aβ and IBO co-injection induced a marked depletion of ChAT activity in the AD control animals compared with sham control. The NP-NAP and Lf-NP-NAP treatment alleviated the decline in a dose-dependent manner, in which the Lf-NP-NAP (0.1 μg/day) group exhibited a ChAT activity 99 ± 8.2% to that of sham control.

3.4.3. Histology

HE staining was used to qualitatively evaluate the neuroprotective effect of NAP formulations on mice hippocampus (Fig. 9). A gross morphological difference was observed between the sham control (Fig. 9A) and the AD control animals (Fig. 9B). Neuron nuclear shrink and karyolysis were observed in CA1 region of hippocampus in the AD control mice, ameliorated following the NAP treatments in the order: 0.05 μg/mouse/d NAP solution group <0.1 μg/mouse/d NAP solution group <0.05 μg/mouse/d NP-NAP <0.1 μg/mouse/d NP-NAP group. Reduced neuronal cell density was also observed in the CA1 region of those mice treated with NAP solution and NP-NAP. In contrast, no gross lesions were observed in the animals treated with Lf-NP-NAP (0.05 μg/day) and Lf-NP-NAP (0.1 μg/day). In addition, Nissl staining cell counting showed that the NP-NAP and Lf-NP-NAP-treated groups exhibited an amelioration of neuronal loss in CA1 region of hippocampus in a dose-dependent manner (Fig. 10).

4. Discussion

AD is the most common neurodegenerative disorder that causes dementia among the elderly. However, the development of new therapeutics for the symptomatic and disease-modifying treatment of AD has been limited by the BBB.

In recent years, the non-invasive intranasal delivery of therapeutic agents bypassing the BBB with drug carriers has drawn a lot of attention [5]. The particular anatomical, physiological and histological characteristics of the nasal cavity enable the direct nose-to-brain drug delivery following intranasal administration. However, it still presents some limitations such as poor membrane penetration, rapid mucociliary clearance, rapid enzymatic degradation and P-gp-mediated efflux [46]. To overcome these difficulties, a variety of strategies are under development, among which pegylated polymeric NPs are promising candidates that can improve drug absorption by protecting drugs against enzymatic degradation and extracellular transportation by P-gp efflux proteins [46,47]. Previous studies showed that surface modification of the nanoparticles with biorecognitive ligands such as lectins (wheat germ agglutinin (WGA), ulex europaeus agglutinin-1 (UEA-1), and Odorranalectin) [33,48,49] and cell-penetrating peptides (CPPs) (low molecular weight protamine (LMWP) and Tat) [40,50] allowed for enhanced brain delivery with reduced clearance and

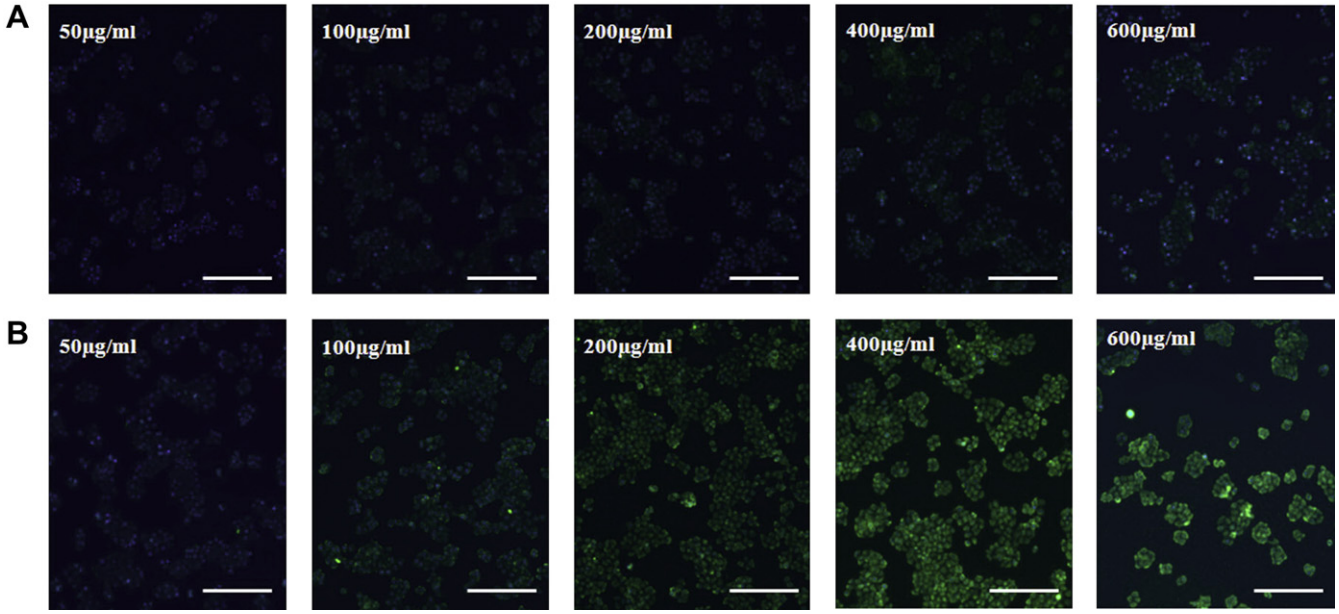

Fig. 2. Cellular uptake of NP (A) and Lf-NP (B) at 37 °C after 1 h incubation at different nanoparticle concentrations. Green, coumarin-6-loaded nanoparticles; Blue, cell nuclei stained with DAPI. The bar is 100 μm. (For interpretation of the references to color in this figure legend, the reader is referred to the web version of this article.)

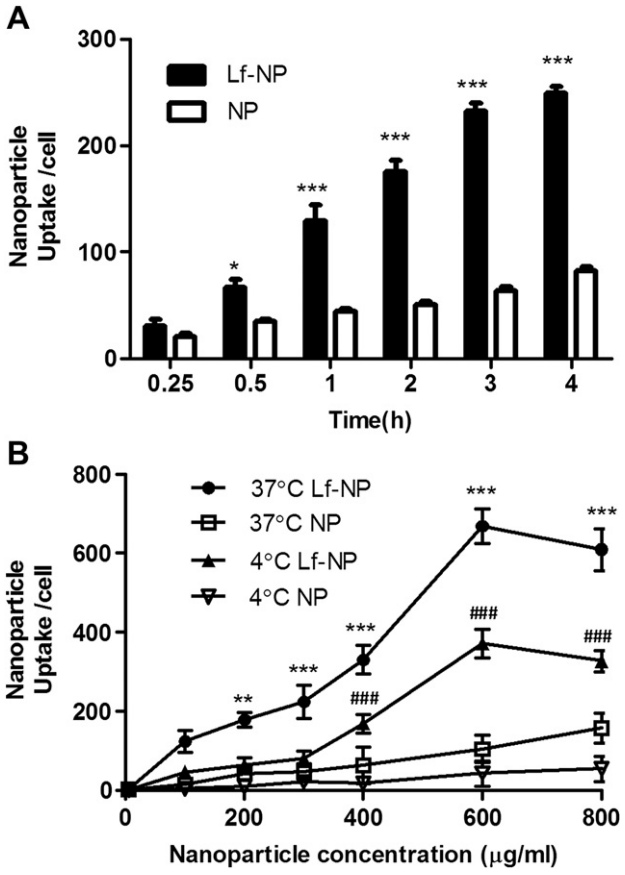

Fig. 3. Cellular uptake of coumarin-6-loaded nanoparticles in 16HBE14o-cells. (A) The cells were incubated with Lf-NP and NP (200 μg/ml) at 37 °C for 15, 30, 60, 120, 180 and 240 min, respectively. (B) The cells were incubated with Lf-NP and NP (5–800 μg/ml) for 1 h at 37 °C and 4 °C, respectively. $^{**}p < 0.01$, $^{***}p < 0.001$ significantly different with that of NP at 37 °C; $^{\#\#\#}p < 0.001$, significantly different with that of NP at 4 °C.

improved absorption [10,47]. However, the use of lectins may be toxic to mammalian cells [51]. WGA-NP has been claimed to induce slight excitotoxicity and oxidative stress, and its long-term toxicity still need to be further studied [52]. The application of Tat-mediated nose-to-brain delivery may induce cargo-dependent cytotoxicity [53,54]. LMWP, which is claimed to be non-cytotoxic, may still harm the normal tissue due to its lack of cell type selectivity [55]. Lf, a naturally occurring ligand, biodegradable, non-toxic and non-immunogenic [56], with its receptor highly expressed on respiratory epithelial cells [19], and also in the brain endothelial cells and neurons [20,21], might serve as an alternative to lectins and CPPs to improve the nose-to-brain drug delivery.

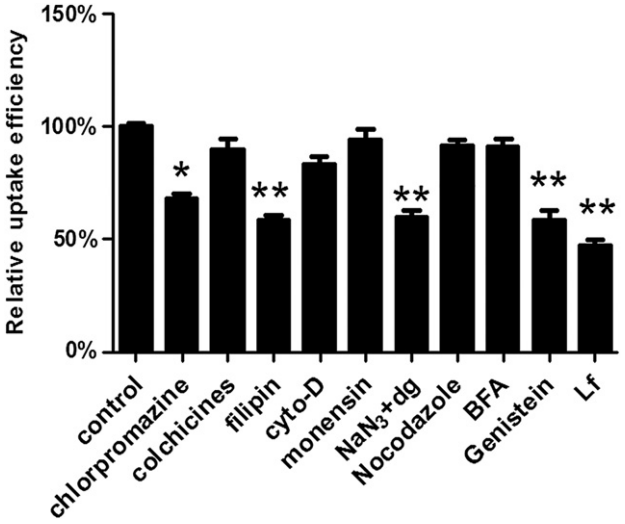

Fig. 4. Cellular uptake of coumarin-6-loaded Lf-NP in the presence of different endocytosis inhibitors (chlorpromazine, colchicines, filipin, cyto-D, monensin, NaN_3 + deoxyglucose, Nocodazole, BFA, Genistein and Lf). Data represent mean ± SD, $n = 3$, $^{*}p < 0.05$, $^{**}p < 0.01$ significantly different with that of the non-inhibited control.

Here we evaluate the potential of Lf-NP as an intranasal DDS for the treatment of AD. Using NAP as a model drug, we studied the neuroprotective effect of Lf-NP-NAP in AD animal models that established by intracerebroventricular co-injection of $A\beta_{1-40}$ and IBO.

According to the previously reported nanoparticle systems for intranasal administration [33,40,57], particle size played an important role in the delivery of nanoparticles from nasal passages to brain. NP and Lf-NP obtained in this study showed diameters less than 90 nm, which was beneficial for nose-to-brain drug delivery. The existence of Lf on the surface of Lf-NP was verified by the CBQCA Protein Quantitation and XPS analysis.

Consistent with previous researches [40,58], *in vitro* release study conducted in pH 4.0 and pH 7.4 showed that almost all the coumarin-6 remained in nanoparticles during the experimental period (data not shown), indicating that the fluorescent signal of coumarin-6 could represent the fate of nanoparticles both *in vitro* and *in vivo*.

Following intranasal administration, the first barrier needed to be overcome is the nasal epithelial cells interconnected by tight junction. 16HBE14o-cells, an immortalized human bronchial epithelial cell line, was here used as the nasal epithelial cell model as previous study showed that little difference in morphology, ciliary activity and high LfR expression was observed between the nasal and bronchial epithelial cells [59]. The uptake of Lf-NP by 16HBE14o-cells was much higher than that of NP, as shown in Fig. 3, indicating that Lf-NP exhibited better cellular uptake. The time, concentration and temperature-dependent cellular uptake pattern of both Lf-NP and NP indicated an active endocytotic process [60].

To elucidate the epithelial cellular interaction mechanism of Lf-NP, the effects of ATP depletion, endocytosis inhibitors and lactoferrin on cellular uptake of Lf-NP were performed quantitatively. Cells treated with NaN_3 + deoxyglucose showed a significant decrease ($p < 0.05$) in cellular uptake (Fig. 4), together with the reduced cellular uptake of Lf-NP at 4 °C (Fig. 3B), indicating that the cellular interaction with Lf-NP was an energy-dependent process.

Understanding the different mechanisms of endocytosis evolved in the interaction between Lf-NP and 16HBE14o-cells would be a key step to drug delivery. One hour pre-incubation with chlorpromazine resulted a significant decrease ($p < 0.05$) in cellular uptake of Lf-NP compared with that of the non-inhibited control (Fig. 4), indicating that clathrin-mediated endocytosis was involved in the cellular uptake of Lf-NP. The cellular uptake of Lf-NP was also inhibited by filipin and genistein (Fig. 4), both of which are typical agents disrupting caveolae [37], suggesting that the cellular import of Lf-NP could be also mediated by caveolae. Besides, cellular uptake still occurred, although reduced, at low temperature (4 °C), indicating an energy-independent direct translocation was involved as well. Lactoferrin was used to investigate the receptor blocking effect, showing that free lactoferrin competitively reduced the epithelial cellular uptake of Lf-NP, which suggested the internalization of Lf-NP involved lactoferrin receptor-mediated endocytosis.

The Lf-mediated brain targeting ability was evaluated by a real-time brain distribution analysis under an *in vivo* imaging system at 0.25 h–3 h after intranasal administration. BSA, a protein shows

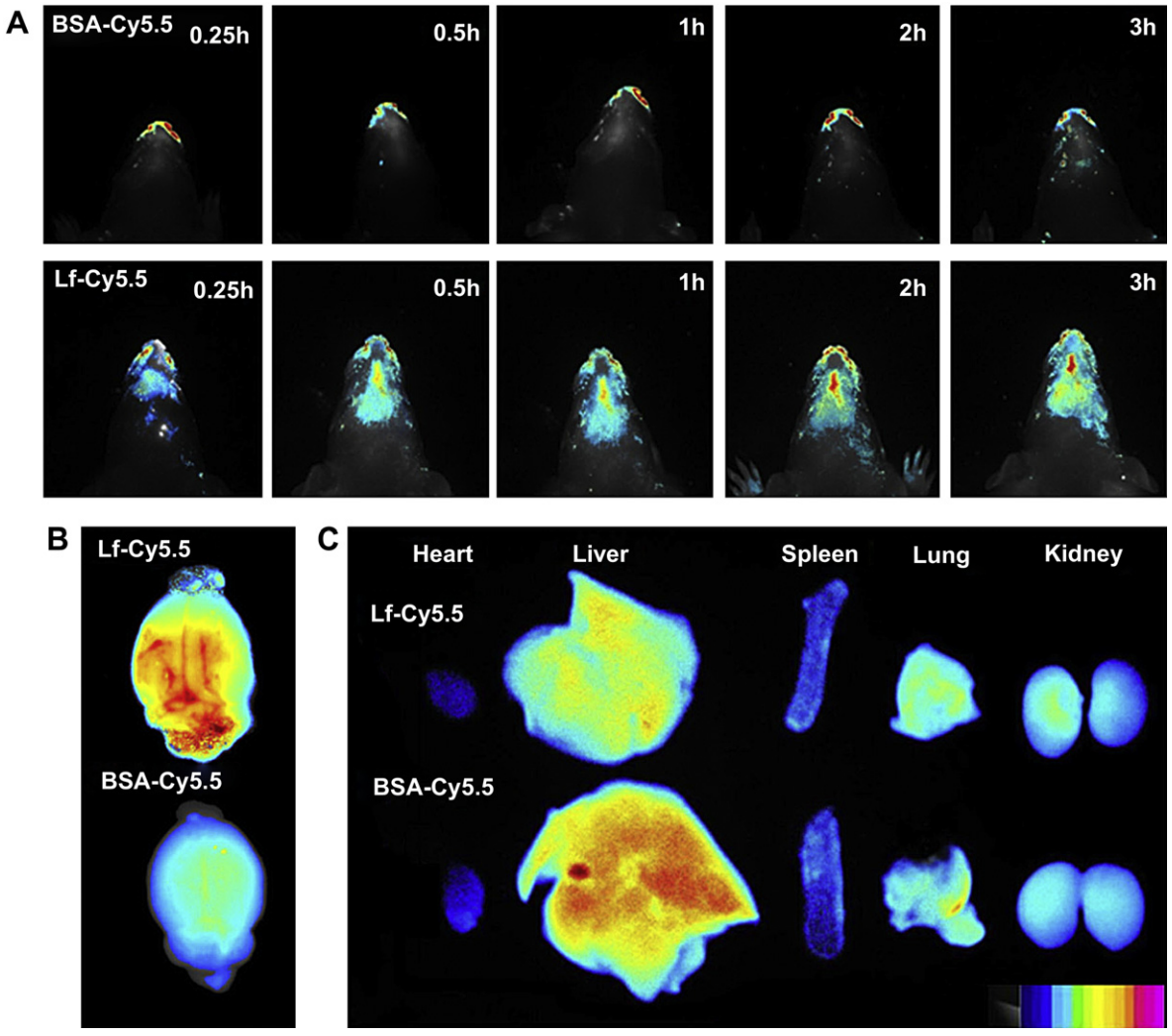

Fig. 5. (A) Distribution and retention of Cy5.5-Lf in the brain following intranasal administration. Distribution of Cy5.5-Lf in (B) brain and (C) main organs following intranasal administration.

no brain targeting ability, was used as the negative control. Fluorescent signals from Cy5.5-Lf was detected in the animal's brain during the whole experimental period while that from Cy5.5-BSA was even not detected (Fig. 5A), indicating that Lf possessed higher efficiency for brain accumulation. In contrast, the fluorescent signal from Cy5.5-BSA was mainly distributed to the liver, lung and spleen when compared with Cy5.5-Lf (Fig. 5B and C), which might be attributed to by its non-specific capture by the mononuclear phagocyte system [61].

Systemic pharmacokinetics and biodistribution of coumarin-6 were determined following intranasal administration of coumarin-6-loaded Lf-NP and NP. The plasma concentration-time curve of Lf-NP and NP were similar (Fig. 6A), suggesting that the conjugation of Lf on the surface of NP did not impair the long-circulation characteristic of PEG. Rapid and significantly increased accumulation of fluorescence tracer (expressed as AUC_{0-8h} and C_{max}) embedded in Lf-NP was obtained in the various brain areas (olfactory bulb, olfactory tract, cerebrum with hippocampus removed, cerebellum and hippocampus) when compared with that in the NP (Table 2), indicating that Lf-NP may contributed to higher transmucosal transport, therefore facilitated higher accumulation of Lf-NP in the brain. The enhanced AUC_{brain}/AUC_{blood} ratio achieved by coumarin-6-loaded Lf-NP (Table 2) also justified the brain-targeting delivery efficiency of Lf-NP. The accumulation was also increased in the hippocampus (Table 2), which makes Lf-NP extremely useful as drug carrier for improving learning and memory [62].

The precise pathways and mechanisms by which a drug travels from the nasal epithelium to various regions of the CNS have not been fully elucidated. The central distribution of ^{125}I-labeled proteins following intranasal administration in rats and monkeys has suggested that delivery occurs along both olfactory and trigeminal nerve pathways [63,64]. It has been demonstrated that transport via the trigeminal nerve pathway facilitated nose-to-brain delivery to caudal brain areas. In contrast, drug directly entered the rostral brain regions via the olfactory pathway [47]. Here, the rank order of coumarin-6 distribution (expressed as AUC_{0-8h}) throughout the brain was: cerebrum with hippocampus removed $\approx$ hippocampus $\approx$ cerebellum $>$ olfactory bulb $>$ olfactory tract, suggesting that after intranasal administration, the nanoparticles might be directly transport to the brain via both the olfactory and the trigeminal nerves pathway. In addition to these direct nose-to-brain transport, those Lf-NP absorbed into the blood circulation might also contribute to enhanced brain delivery as LfR was also highly expressed in brain endothelial cells [20,21] and has been proved efficient in facilitating the brain delivery of nanoparticulate DDS [17].

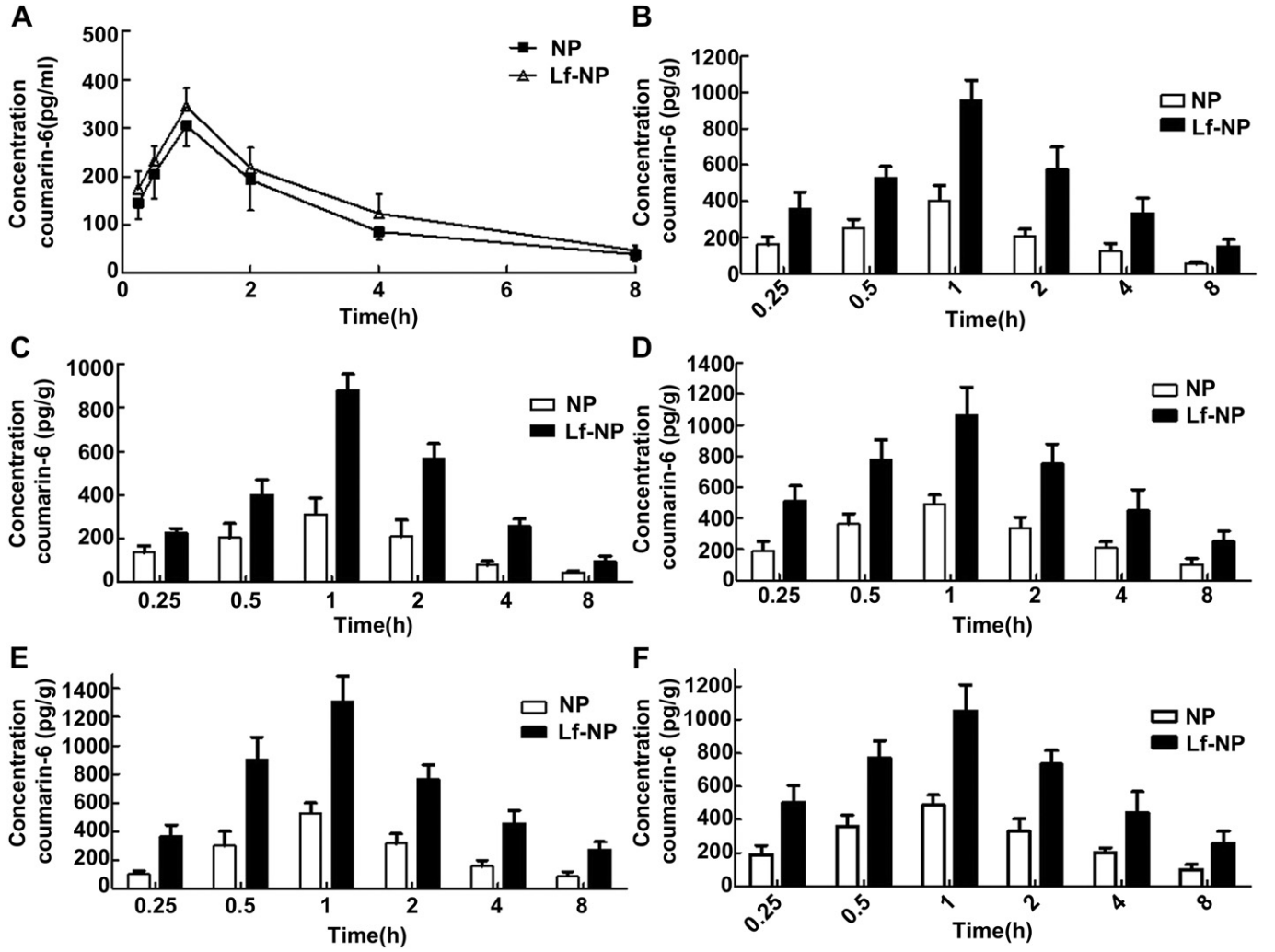

Fig. 6. (A) Blood concentration-time profiles of coumarin-6 following intranasal administration of coumarin-6 loaded Lf-NP and NP. Data represented the mean ± S.D. $n = 3$. Brain biodistribution of coumarin-6 following intranasal administration of coumarin-6-loaded Lf-NP and NP in the (B) olfactory bulb, (C) olfactory tract, (D) cerebrum with hippocampus removed, (E) cerebellum and (F) hippocampus.

However, increased AUC_{brain}/AUC_{blood} and $C_{max,\ brain}/C_{max,\ blood}$ ratio of coumarin-6-loaded Lf-NP were achieved following intranasal administration *vs.* intravenous administration [17], suggesting that the increased brain accumulation of coumarin-6 after nasal delivery of Lf-NP was largely contributed by the direct nose-to-brain transport other than the vasculature pathway. Furthermore, our pharmacokinetic data showed that enhanced brain delivery is clearly seen within 1 h, indicating that rapid extracellular delivery might largely contributed to the brain delivery since intracellular delivery involving axonal transport would require a much longer period of time [65]. Therefore, we concluded that the enhanced brain delivery following Lf-NP intranasal administration was very likely largely achieved via both the olfactory and the trigeminal nerves pathway in a the rapid extracellular delivery manner.

Table 2
Pharmacokinetic parameters of coumarin-6 following an intranasal administration of labeled Lf-NP and NP.

Formulation	Tissue	C_{max} (pg/ml or pg/g)	T_{max} (h)	AUC_{0-8h} (pg h/ml or pg h/g)	AUC_{brain}/AUC_{blood}
Lf-NP	Blood	344.69	1	1180.10	–
	OB	957.17***	1	3179.18***	2.69***
	OT	880.95***	1	2679.98***	2.27***
	CR	1307.85***	1	4484.86***	3.80***
	CL	1067.07***	1	4212.75***	3.57***
	HI	1053.25***	1	4143.74***	3.51***
NP	Blood	305.10	1	966.49	–
	OB	402.54	1	1238.44	1.28
	OT	312.82	1	993.90	1.03
	CR	490.53	1	1901.42	1.97
	CL	531.10	1	1663.84	1.72
	HI	486.10	1	1854.70	1.92

OB, olfactory bulb; OT, olfactory tract; CR, cerebrum with hippocampus removed; CL, cerebellum; HI, hippocampus. ***$p < 0.001$ significant different with that of NP.

Accumulating evidence suggests that the co-injection of $A\beta_{1\text{-}40}$ with a small amount of IBO produced drastic neuronal loss, which provides a useful model for studying the pathogenetic mechanisms leading to AD [66–68]. In order to evaluate the neuroprotective effect of Lf-NP-NAP, we here use mice intracerebroventricularly co-injected with preaggregated $A\beta_{1-40}$ and a small amount of IBO as the animal model [42].

MWM described thirty years ago has become one of the most frequently laboratory tools to study the neurocognitive disorders. In this study, we applied the basic training protocols including four days hidden-platform acquisition training and a probe trial testing on day five. During the first four days hidden-platform acquisition phase of the MWM task, we analyzed the escape latency (time required to reach the platform) as a standard performance

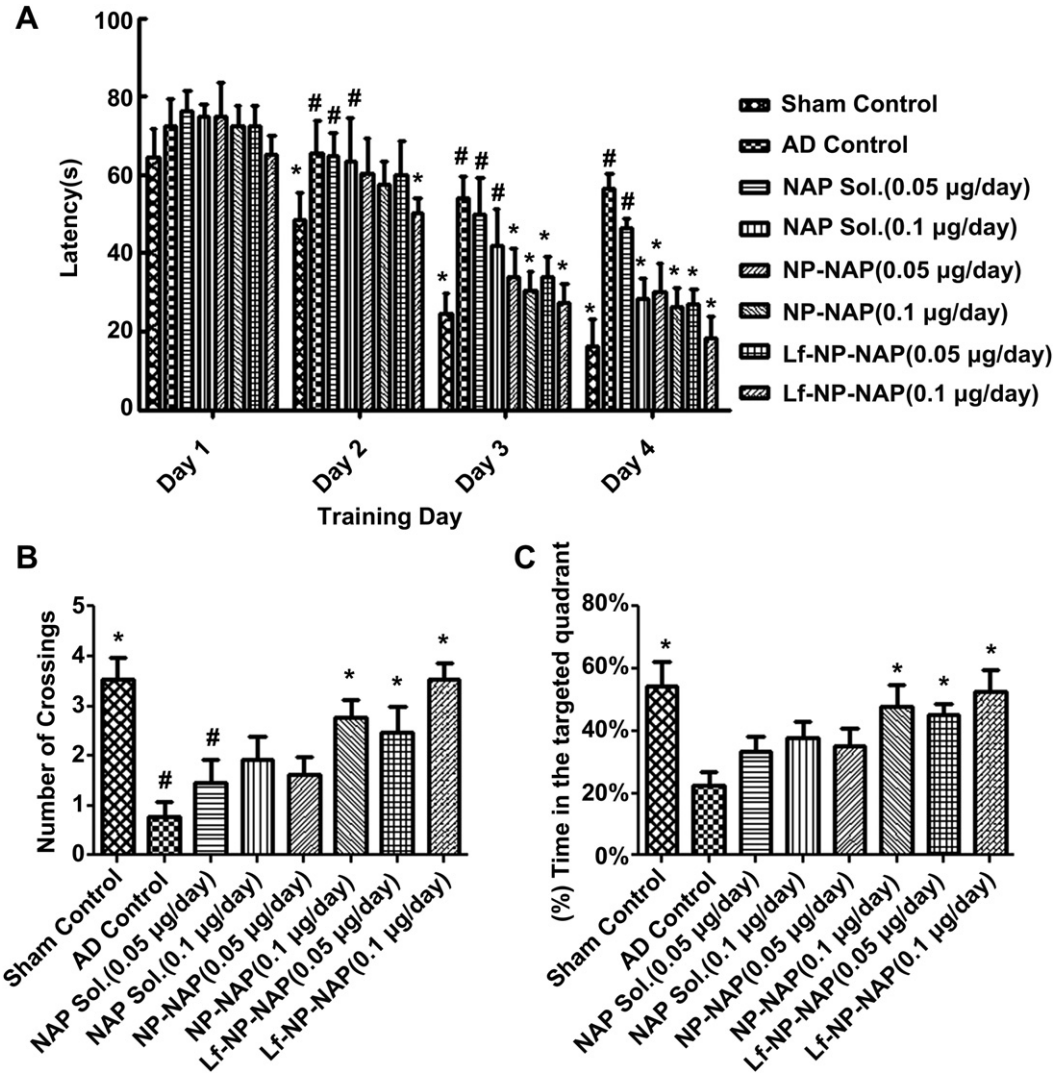

Fig. 7. (A) Neuroprotection effects of nasal administration of NAP solution, NP-NAP, and Lf-NP-NAP on the impairment of water maze learning in mice with lesions induced by intracerebroventricular co-injection with $A\beta_{1-40}$ and IBO. Training began after 34 days of recovering and daily drug application. Data represented the mean ± S.E.M.; (B) Effects of nasal administration of NAP solution, NP-NAP and Lf-NP-NAP on the number of times crossed the area where the platform had been located. Day 5 of testing, a spatial probe test performed with the platform removed. The animals allowed swim for 60 s, and the mean number of times the animals crossed the area where the platform had been located recorded. Data represented the mean ± S.E.M.; (C) the percent of (%) time in the targeted quadrant where the platform had been located. Data represented the mean ± S.E.M. ($n = 8$). $^{*}p < 0.05$, significantly different from AD control; $^{\#}p < 0.05$, significantly different from sham control. Sham control, given saline instead of $A\beta_{1-40}$ and IBO and received daily applied saline; AD control, daily applied saline; NAP Sol. (0.05 μg/day), intranasal administration of NAP solution at the dose of 0.05 μg/mouse/day NAP; NAP Sol. (0.1 μg/day), intranasal administration of NAP solution at the dose of 0.1 μg/mouse/day NAP; NP-NAP (0.05 μg/day), intranasal administration of NP-NAP at the dose of 0.05 μg/mouse/day NAP; NP-NAP (0.1 μg/day), intranasal administration of NP-NAP at the dose of 0.1 μg/mouse/day NAP; Lf-NP-NAP (0.05 μg/day), intranasal administration of Lf-NP-NAP at the dose of 0.05 μg/mouse/day NAP; Lf-NP-NAP (0.1 μg/day), intranasal administration of Lf-NP-NAP at the dose of 0.1 μg/mouse/day NAP.

measure [69]. Results from the AD control group indicated that intracerebroventricular co-injection of $A\beta_{1-40}$ and IBO induced learning and memory dysfunction in mice. Animals treated with the NP formulations showed amelioration in cognitive deficits in a dose-dependent manner: the most significant decrease in latency on day 2, 3, and 4 was observed following intranasal administration of 0.1 μg of NAP that loaded by Lf-NP, but only on day 3 and 4 after the administration of other formulations. These results were confirmed by the number of times crossing the area where the platform had been located and the percentage of time spent in the target quadrant. Intranasal administration of Lf-NP-NAP provided a significant improvement in the MWM task even at a very low drug dose (0.05 μg).

Maintaining normal function of cholinergic neurotransmitter system is important for brain function, which requires the balance between activity of AChE (the enzyme that degrades acetylcholine) and activity of ChAT (the enzyme that synthesizes acetylcholine). Evidence from a variety of sources implicated that Aβ-induced deficits in cholinergic neurotransmission [70–72], and led to deficits in learning, memory and other aspects of cognition. Former study showed that NAP protected animals from loss of cholinergic functions [31]. In this contribution, the NAP-related neuroprotection was also studied by determining the activity of AChE and ChAT in the mice hippocampus. It was showed that Lf-NP-NAP also protected the model animals against Aβ-induced inhibition of ChAT and increase of AchE activity even at the dose (0.05 μg) half of that of NP-NAP (0.1 μg) (Fig. 8A and B). These studies suggest that Lf-NP might provide a more efficacious drug delivery system than unmodified NP and drug solution.

As indicated above, co-injection of $A\beta_{1-40}$ and IBO could induce a synergistic loss of hippocampal neurons [67,68], which might be ameliorated by NAP treatment [73]. In our study, we used HE

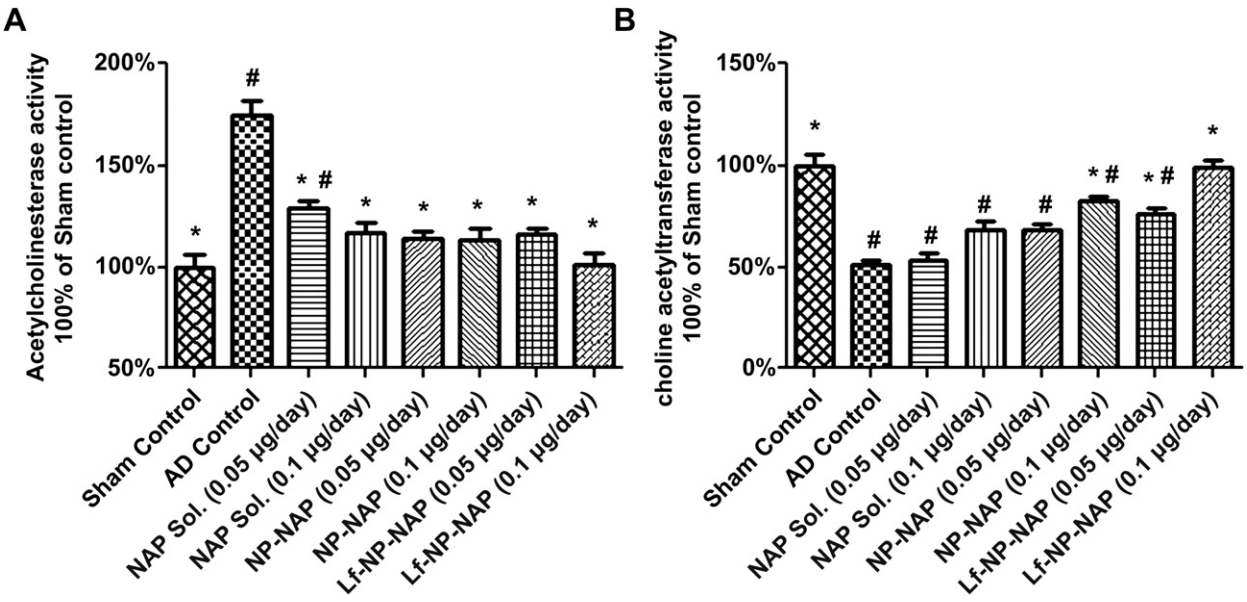

Fig. 8. Intranasal application of Lf-NP-NAP nanoparticles prevented inhibition of ChAT and increase of AChE activity in mice. (A) AChE and (B) ChAT activity in the hippocampus of mice intracerebroventricular co-injection with $A\beta_{1-40}$ and IBO. Results were calibrated against sham control (100%). Data represented the mean ± S.E.M. ($n = 5$). $^{*}p < 0.05$, significantly different from AD control; $^{\#}p < 0.05$, significantly different from sham control.

staining to determine different cellular and microanatomical features between normal and the injured brains. Both gross morphology observation and quantitative cell counting results showed that none visible damages were detected in the brain of mice treated with Lf-NP-NAP even in a lower drug dose (0.05 μg) compared to other formulations. The neuroprotection effect of Lf-NP-NAP demonstrated here was superior to that of other formulations.

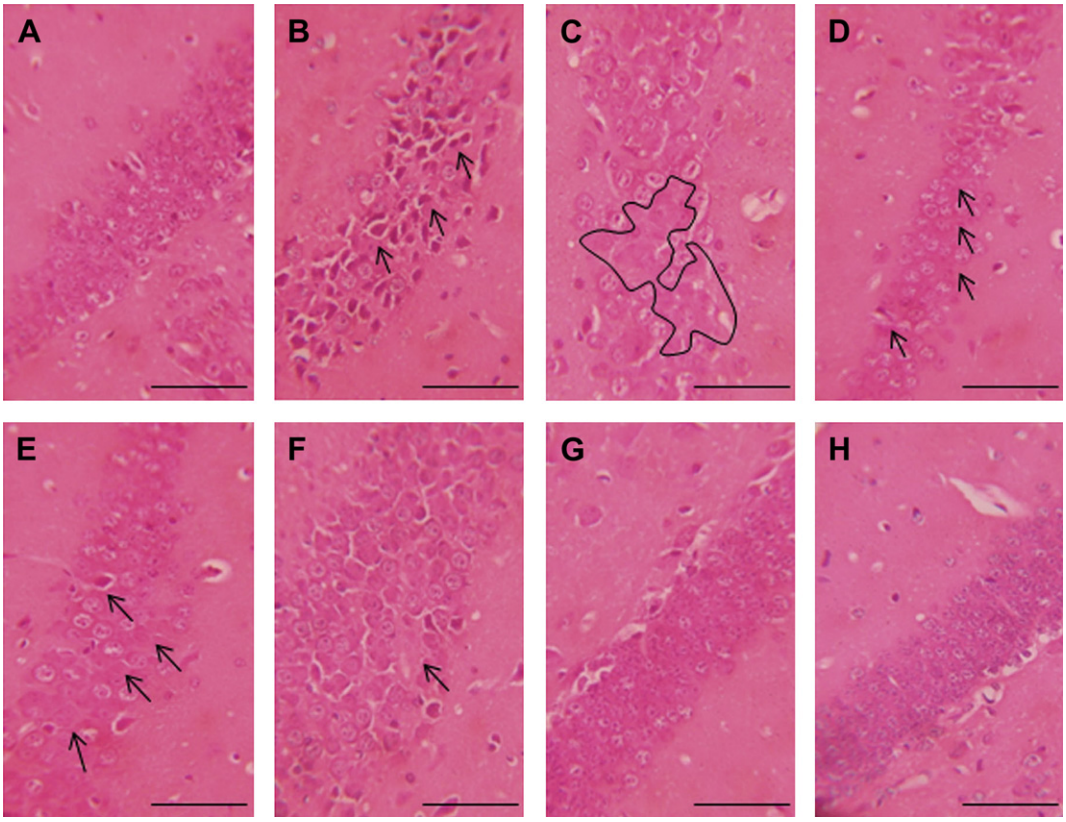

Fig. 9. HE staining in the CA1 region of right hippocampus from mice treated with: (A) sham control; (B) AD control; (C) i.n. NAP Sol. (0.05 μg/day); (D) i.n. NAP Sol. (0.1 μg/day); (E) i.n. NP-NAP (0.05 μg/day); (F) i.n. NP-NAP (0.1 μg/day); (G) i.n. Lf-NP-NAP (0.05 μg/day); and (H) i.n. Lf-NP-NAP (0.1 μg/day). Scale Bar, 25 μm. Arrows show neuronal damage in hippocampus in B, D, E and F. Black polygon shows neuronal damage in hippocampus in C.

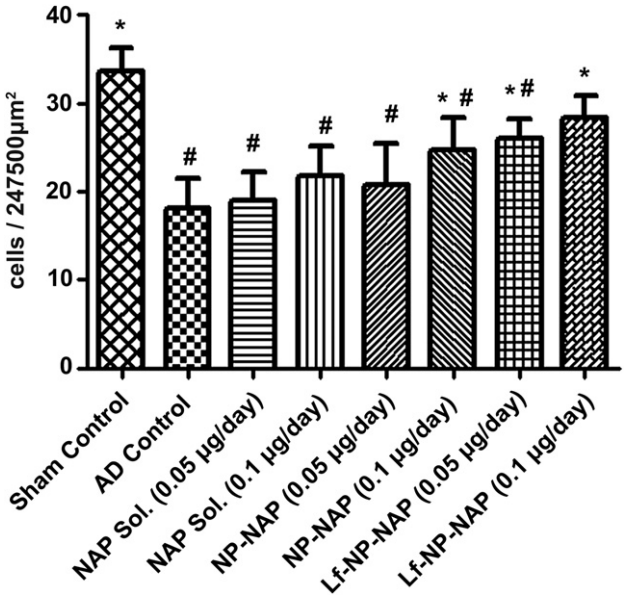

Fig. 10. Neuroprotective effects of nasal administration of NAP solution, NP-NAP, and Lf-NP-NAP on the neuronal loss in the hippocampus CA1 region of mice with lesions induced by co-injection of $A\beta_{1-40}$ and IBO. Number of neurons in mice CA1 region after 35 days of daily drug application (cells/247,500 μm^2, $n = 15$). Data represented the mean ± S.D. $^{*}p < 0.05$, significantly different from AD control; $^{\#}p < 0.05$, significantly different from sham control.

5. Conclusion

In this study, we proposed PEG-PCL nanoparticles modified with lactoferrin as an effective intranasal DDS in mediating NAP transport into the brain for the treatment of Alzheimer's disease. Cellular experiments showed that Lf-NP exhibited significantly enhanced cellular accumulation than that of unmodified NP via clathrin-/caveolae-mediated endocytosis and direct translocation. It also exhibited a desirable brain biodistribution profile with significantly increased coumarin-6 delivery in the rat olfactory bulb, olfactory tract, hippocampus, cerebellum and cerebrum with hippocampus removed. In the pharmacodynamic experiment, Lf-NP-NAP treatment showed significant improvement in both behavioral studies and in histology study. These results definitely indicated that the DDS described here could offer an effective non-invasive approach to facilitate the access of neuropeptides to the CNS.

Acknowledgments

This work was supported by National Natural Science Foundation of China (81072592), National Key Basic Research Program (2010CB529800), National Science and Technology major Project (2012ZX09304004), Program for New Century Excellent Talents in University, Grants from Shanghai Science and Technology Committee (11430702200, 12ZR1416300 and 12nm0502000), Innovation Program of Shanghai Municipal Education Commission (12ZZ107) and SJTU Funding (AE4160003).

References

[1] Cvetković-Dožić D, Skender-Gazibara M, Dožić S. Neuropathological hallmarks of Alzheimer's disease. Arch Oncol 2001;9:195–9.
[2] Ferri CP, Prince M, Brayne C, Brodaty H, Fratiglioni L, Ganguli M, et al. Global prevalence of dementia: a Delphi consensus study. Lancet 2005;366:2112–7.
[3] Smith MA. Alzheimer disease. Int Rev Neurobiol 1998;42:1–54.
[4] Kuljis RO, Salkovic-Petrisic M. Dementia, diabetes, Alzheimer's disease, and insulin resistance in the brain: progress, dilemmas, new opportunities, and a hypothesis to tackle intersecting epidemics. J Alzheimers Dis 2011;25:29–41.
[5] Malerba F, Paoletti F, Capsoni S, Cattaneo A. Intranasal delivery of therapeutic proteins for neurological diseases. Expert Opin Drug Deliv 2011;8:1277–96.
[6] Hanson LR, Frey WN. Intranasal delivery bypasses the blood-brain barrier to target therapeutic agents to the central nervous system and treat neurodegenerative disease. BMC Neurosci 2008;9(Suppl. 3):S5.
[7] Thorne RG, Emory CR, Ala TA, Frey WN. Quantitative analysis of the olfactory pathway for drug delivery to the brain. Brain Res 1995;692:278–82.
[8] Illum L. Is nose-to-brain transport of drugs in man a reality? J Pharm Pharmacol 2004;56:3–17.
[9] Danielyan L, Schafer R, von Ameln-Mayerhofer A, Bernhard F, Verleysdonk S, Buadze M, et al. Therapeutic efficacy of intranasally delivered mesenchymal stem cells in a rat model of Parkinson disease. Rejuvenation Res 2011;14:3–16.
[10] Dhuria SV, Hanson LR, Frey WN. Intranasal delivery to the central nervous system: mechanisms and experimental considerations. J Pharm Sci 2010;99:1654–73.
[11] Schioth HB, Craft S, Brooks SJ, Frey WN, Benedict C. Brain insulin signaling and Alzheimer's disease: current evidence and future directions. Mol Neurobiol 2012;46:4–10.
[12] Craft S, Baker LD, Montine TJ, Minoshima S, Watson GS, Claxton A, et al. Intranasal insulin therapy for Alzheimer disease and amnestic mild cognitive impairment: a pilot clinical trial. Arch Neurol 2012;69:29–38.
[13] Ali J, Ali M, Baboota S, Sahani JK, Ramassamy C, Dao L, et al. Potential of nanoparticulate drug delivery systems by intranasal administration. Curr Pharm Des 2010;16:1644–53.
[14] Verma A, Stellacci F. Effect of surface properties on nanoparticle-cell interactions. Small 2010;6:12–21.
[15] Ward PP, Uribe-Luna S, Conneely OM. Lactoferrin and host defense. Biochem Cell Biol 2002;80:95–102.
[16] Nuijens JH, van Berkel PH, Schanbacher FL. Structure and biological actions of lactoferrin. J Mammary Gland Biol Neoplasia 1996;1:285–95.
[17] Hu K, Li J, Shen Y, Lu W, Gao X, Zhang Q, et al. Lactoferrin-conjugated PEG-PLA nanoparticles with improved brain delivery: in vitro and in vivo evaluations. J Control Release 2009;134:55–61.
[18] Huang R, Ke W, Liu Y, Jiang C, Pei Y. The use of lactoferrin as a ligand for targeting the polyamidoamine-based gene delivery system to the brain. Biomaterials 2008;29:238–46.
[19] Elfinger M, Maucksch C, Rudolph C. Characterization of lactoferrin as a targeting ligand for nonviral gene delivery to airway epithelial cells. Biomaterials 2007;28:3448–55.
[20] Suzuki YA, Lopez V, Lonnerdal B. Mammalian lactoferrin receptors: structure and function. Cell Mol Life Sci 2005;62:2560–75.
[21] Legrand D, Pierce A, Elass E, Carpentier M, Mariller C, Mazurier J. Lactoferrin structure and functions. Adv Exp Med Biol 2008;606:163–94.
[22] Qian ZM, Wang Q. Expression of iron transport proteins and excessive iron accumulation in the brain in neurodegenerative disorders. Brain Res Brain Res Rev 1998;27:257–67.
[23] Ji B, Maeda J, Higuchi M, Inoue K, Akita H, Harashima H, et al. Pharmacokinetics and brain uptake of lactoferrin in rats. Life Sci 2006;78:851–5.
[24] Gozes I, Divinsky I, Pilzer I, Fridkin M, Brenneman DE, Spier AD. From vasoactive intestinal peptide (VIP) through activity-dependent neuroprotective protein (ADNP) to NAP: a view of neuroprotection and cell division. J Mol Neurosci 2003;20:315–22.
[25] Gozes I, Steingart RA, Spier AD. NAP mechanisms of neuroprotection. J Mol Neurosci 2004;24:67–72.
[26] Gozes I, Morimoto BH, Tiong J, Fox A, Sutherland K, Dangoor D, et al. NAP: research and development of a peptide derived from activity-dependent neuroprotective protein (ADNP). Cns Drug Rev 2005;11:353–68.
[27] Bassan M, Zamostiano R, Davidson A, Pinhasov A, Giladi E, Perl O, et al. Complete sequence of a novel protein containing a femtomolar-activity-dependent neuroprotective peptide. J Neurochem 1999;72:1283–93.
[28] Zemlyak I, Furman S, Brenneman DE, Gozes I. A novel peptide prevents death in enriched neuronal cultures. Regul Pept 2000;96:39–43.
[29] Beni-Adani L, Gozes I, Cohen Y, Assaf Y, Steingart RA, Brenneman DE, et al. A peptide derived from activity-dependent neuroprotective protein (ADNP) ameliorates injury response in closed head injury in mice. J Pharmacol Exp Ther 2001;296:57–63.
[30] Wilkemeyer MF, Chen SY, Menkari CE, Brenneman DE, Sulik KK, Charness ME. Differential effects of ethanol antagonism and neuroprotection in peptide fragment NAPVSIPQ prevention of ethanol-induced developmental toxicity. Proc Natl Acad Sci U S A 2003;100:8543–8.
[31] Gozes I, Giladi E, Pinhasov A, Bardea A, Brenneman DE. Activity-dependent neurotrophic factor: intranasal administration of femtomolar-acting peptides improve performance in a water maze. J Pharmacol Exp Ther 2000;293:1091–8.
[32] Illum L. Nasal drug delivery–possibilities, problems and solutions. J Control Release 2003;87:187–98.
[33] Gao X, Tao W, Lu W, Zhang Q, Zhang Y, Jiang X, et al. Lectin-conjugated PEG-PLA nanoparticles: preparation and brain delivery after intranasal administration. Biomaterials 2006;27:3482–90.
[34] Huwyler J, Wu D, Pardridge WM. Brain drug delivery of small molecules using immunoliposomes. Proc Natl Acad Sci U S A 1996;93:14164–9.
[35] Ellman GL. Tissue sulfhydryl groups. Arch Biochem Biophys 1959;82:70–7.

[36] Olivier JC, Huertas R, Lee HJ, Calon F, Pardridge WM. Synthesis of pegylated immunonanoparticles. Pharm Res 2002;19:1137–43.
[37] Xin H, Sha X, Jiang X, Chen L, Law K, Gu J, et al. The brain targeting mechanism of Angiopep-conjugated poly(ethylene glycol)-co-poly(epsilon-caprolactone) nanoparticles. Biomaterials 2012;33:1673–81.
[38] Gao X, Wang T, Wu B, Chen J, Chen J, Yue Y, et al. Quantum dots for tracking cellular transport of lectin-functionalized nanoparticles. Biochem Biophys Res Commun 2008;377:35–40.
[39] Guo J, Gao X, Su L, Xia H, Gu G, Pang Z, et al. Aptamer-functionalized PEG-PLGA nanoparticles for enhanced anti-glioma drug delivery. Biomaterials 2011;32:8010–20.
[40] Xia H, Gao X, Gu G, Liu Z, Zeng N, Hu Q, et al. Low molecular weight protamine-functionalized nanoparticles for drug delivery to the brain after intranasal administration. Biomaterials 2011;32:9888–98.
[41] Tran MH, Yamada K, Nabeshima T. Amyloid beta-peptide induces cholinergic dysfunction and cognitive deficits: a minireview. Peptides 2002;23:1271–83.
[42] Van Dam D, De Deyn PP. Drug discovery in dementia: the role of rodent models. Nat Rev Drug Discov 2006;5:956–70.
[43] Kihara T, Shimohama S. Alzheimer's disease and acetylcholine receptors. Acta Neurobiol Exp (Wars) 2004;64:99–105.
[44] Li J, Huang H, Miezan EJ, Gao XL, Massicot F, Dong CZ, et al. Pharmacological profile of PMS777, a new AChE inhibitor with PAF antagonistic activity. Int J Neuropsychopharmacol 2007;10:21–9.
[45] Holmes GL, Gairsa JL, Chevassus-Au-Louis N, Ben-Ari Y. Consequences of neonatal seizures in the rat: morphological and behavioral effects. Ann Neurol 1998;44:845–57.
[46] Pires A, Fortuna A, Alves G, Falcao A. Intranasal drug delivery: how, why and what for? J Pharm Pharm Sci 2009;12(3):288–311.
[47] Mistry A, Stolnik S, Illum L. Nanoparticles for direct nose-to-brain delivery of drugs. Int J Pharm 2009;379:146–57.
[48] Gao X, Chen J, Tao W, Zhu J, Zhang Q, Chen H, et al. UEA I-bearing nanoparticles for brain delivery following intranasal administration. Int J Pharm 2007;340:207–15.
[49] Wen Z, Yan Z, Hu K, Pang Z, Cheng X, Guo L, et al. Odorranalectin-conjugated nanoparticles: preparation, brain delivery and pharmacodynamic study on Parkinson's disease following intranasal administration. J Control Release 2011;151:131–8.
[50] Kanazawa T, Taki H, Tanaka K, Takashima Y, Okada H. Cell-penetrating peptide-modified block copolymer micelles promote direct brain delivery via intranasal administration. Pharm Res 2011;28:2130–9.
[51] Reynoso-Camacho R, Gonzalez DME, Loarca-Pina G. Purification and acute toxicity of a lectin extracted from tepary bean (Phaseolus acutifolius). Food Chem Toxicol 2003;41:21–7.
[52] Liu Q, Shao X, Chen J, Shen Y, Feng C, Gao X, et al. In vivo toxicity and immunogenicity of wheat germ agglutinin conjugated poly(ethylene glycol)-poly(lactic acid) nanoparticles for intranasal delivery to the brain. Toxicol Appl Pharmacol 2011;251:79–84.
[53] El-Andaloussi S, Jarver P, Johansson HJ, Langel U. Cargo-dependent cytotoxicity and delivery efficacy of cell-penetrating peptides: a comparative study. Biochem J 2007;407:285–92.
[54] Kilk K, Mahlapuu R, Soomets U, Langel U. Analysis of in vitro toxicity of five cell-penetrating peptides by metabolic profiling. Toxicology 2009;265:87–95.
[55] Koren E, Torchilin VP. Cell-penetrating peptides: breaking through to the other side. Trends Mol Med 2012;18:385–93.
[56] Li H, Sun H, Qian ZM. The role of the transferrin-transferrin-receptor system in drug delivery and targeting. Trends Pharmacol Sci 2002;23:206–9.
[57] Brooking J, Davis SS, Illum L. Transport of nanoparticles across the rat nasal mucosa. J Drug Target 2001;9:267–79.
[58] Gan CW, Feng SS. Transferrin-conjugated nanoparticles of poly(lactide)-D-alpha-tocopheryl polyethylene glycol succinate diblock copolymer for targeted drug delivery across the blood-brain barrier. Biomaterials 2010;31:7748–57.
[59] Devalia JL, Sapsford RJ, Wells CW, Richman P, Davies RJ. Culture and comparison of human bronchial and nasal epithelial cells in vitro. Respir Med 1990;84:303–12.
[60] Allen C, Yu Y, Eisenberg A, Maysinger D. Cellular internalization of PCL(20)-b-PEO(44) block copolymer micelles. Biochim Biophys Acta 1999;1421:32–8.
[61] Li J, Feng L, Fan L, Zha Y, Guo L, Zhang Q, et al. Targeting the brain with PEG-PLGA nanoparticles modified with phage-displayed peptides. Biomaterials 2011;32:4943–50.
[62] Bannerman DM, Rawlins JN, McHugh SB, Deacon RM, Yee BK, Bast T, et al. Regional dissociations within the hippocampus–memory and anxiety. Neurosci Biobehav Rev 2004;28:273–83.
[63] Thorne RG, Pronk GJ, Padmanabhan V, Frey WN. Delivery of insulin-like growth factor-I to the rat brain and spinal cord along olfactory and trigeminal pathways following intranasal administration. Neuroscience 2004;127:481–96.
[64] Thorne RG, Hanson LR, Ross TM, Tung D, Frey WN. Delivery of interferon-beta to the monkey nervous system following intranasal administration. Neuroscience 2008;152:785–97.
[65] Lochhead JJ, Thorne RG. Intranasal delivery of biologics to the central nervous system. Adv Drug Deliv Rev 2012;64:614–28.
[66] Dornan WA, Kang DE, McCampbell A, Kang EE. Bilateral injections of beta A(25-35) + IBO into the hippocampus disrupts acquisition of spatial learning in the rat. Neuroreport 1993;5:165–8.
[67] Morimoto K, Yoshimi K, Tonohiro T, Yamada N, Oda T, Kaneko I. Co-injection of beta-amyloid with ibotenic acid induces synergistic loss of rat hippocampal neurons. Neuroscience 1998;84:479–87.
[68] Ito Y, Ito M, Takagi N, Saito H, Ishige K. Neurotoxicity induced by amyloid beta-peptide and ibotenic acid in organotypic hippocampal cultures: protection by S-allyl-L-cysteine, a garlic compound. Brain Res 2003;985:98–107.
[69] D'Hooge R, De Deyn PP. Applications of the Morris water maze in the study of learning and memory. Brain Res Brain Res Rev 2001;36:60–90.
[70] Oddo S, Caccamo A, Green KN, Liang K, Tran L, Chen Y, et al. Chronic nicotine administration exacerbates tau pathology in a transgenic model of Alzheimer's disease. Proc Natl Acad Sci U S A 2005;102:3046–51.
[71] Kasa PS, Papp H, Kasa PJ, Pakaski M, Balaspiri L. Effects of amyloid-beta on cholinergic and acetylcholinesterase-positive cells in cultured basal forebrain neurons of embryonic rat brain. Brain Res 2004;998:73–82.
[72] Boncristiano S, Calhoun ME, Kelly PH, Pfeifer M, Bondolfi L, Stalder M, et al. Cholinergic changes in the APP23 transgenic mouse model of cerebral amyloidosis. J Neurosci 2002;22:3234–43.
[73] Zemlyak I, Manley N, Sapolsky R, Gozes I. NAP protects hippocampal neurons against multiple toxins. Peptides 2007;28:2004–8.